

# Optics Letters

## Fiber micro-tip temperature sensor based on cholesteric liquid crystal

JIANYANG HU,<sup>1</sup> DONG ZHOU,<sup>1</sup> YUEMING SU,<sup>1</sup> SHUANGQIANG LIU,<sup>2</sup> PEIXIAN MIAO,<sup>3</sup> YANCHAO SHI,<sup>3</sup> WEIMIN SUN,<sup>1</sup>  AND YONGJUN LIU<sup>1,4,\*</sup>

<sup>1</sup>Key Lab of In-fiber Integrated Optics, Ministry Education of China, Harbin Engineering University, Harbin 150001, China

<sup>2</sup>School of Physics and Astronomy, Sun Yat-Sen University, Zhuhai, Guangdong 519082, China

<sup>3</sup>Science and Technology on Vacuum Technology and Physics Laboratory, Lanzhou Institute of Physics, Lanzhou 730000, China

<sup>4</sup>State Key Laboratory of Applied Optics, Changchun Institute of Optics, Fine Mechanics and Physics, Chinese Academy of Sciences, Changchun 130033, China

\*Corresponding author: liuyj@hrbeu.edu.cn

Received 10 July 2020; revised 3 August 2020; accepted 11 August 2020; posted 12 August 2020 (Doc. ID 402473); published 14 September 2020

**This Letter proposes and demonstrates a novel, miniature fiber-tip temperature sensor with a tapered hollow capillary tube (HCT) filled with glycerin and dye-doped cholesteric liquid crystal (CLC). The function of glycerin is to provide a surface anchoring force to control the uniform orientation of CLC molecules, so that the CLC in the tapered HCT can be considered as a mirrorless photonic bandgap (PBG) microcavity. An unambiguously identifiable PBG mode single peak appears in the emission spectra of the sensor. The CLC-based fiber-tip temperature sensor has a temperature sensitivity of  $-9.167 \text{ nm}/^\circ\text{C}$ , and the figure of merit can reach  $67.4^\circ\text{C}^{-1}$ . This sensor offers key features and advantages, including compactness, unambiguous identifiability, and biocompatibility, which can satisfy requirements of temperature measurement in various temperature sensing application fields and has great potential for biochemical detection at cell level. In addition, the CLC was integrated into the optical fiber terminal, and the PBG mode is excited, collected and transmitted by the multimode fiber coupler, which is reported for the first time, to the best of our knowledge.** © 2020 Optical Society of America

<https://doi.org/10.1364/OL.402473>

Fiber-optic temperature sensors have been proposed and widely applied in recent years, but there are still some problems that need to be solved. For example, the fiber grating sensor requires complex and expensive equipment for grating inscription [1]. The fiber modal interference sensor measures the temperature by recognizing the wavelength shift of the sensor spectrum [2,3]. Due to the periodic nature of the spectrum of these sensors, the direction ambiguity is a well-known problem when the wavelength shift of the spectrum is more than half of the free spectral range [4]. In addition, the cross sensitivity of strain has become a problem that cannot be ignored. The micro-structural fiber sensor is limited by the high expense of the specialty fiber and fragile structures [5,6]. In the above structure, the temperature sensitivity is usually not high enough because of the low

thermo-optic coefficient (TOC) and thermal expansion coefficient (TEC) of the silica material. To increase the temperature sensitivity of the fiber sensor, materials with high TOCs and TECs are integrated into fiber-optic sensors. Li *et al.* fabricated a polymer micro-structure within the SU-8 photoresist, and the liquid polymer was sealed in the micro-structure [7]. The temperature sensitivity of the proposed sensor was  $877 \text{ pm}/^\circ\text{C}$ . As a material with a high birefringence and high temperature sensitivity, liquid crystal (LC) has been comprehensively used in fiber temperature sensors. Dora *et al.* selectively filled the nematic LC into a single void within the photonic crystal fiber structure and obtained the temperature sensitivity of  $3.9 \text{ nm}/^\circ\text{C}$  [8]. In our previous work, we proposed a Fabry–Perot interferometer temperature sensor based on LC and the Vernier effect, and the proposed sensor can provide a temperature sensitivity of  $19.55 \text{ nm}/^\circ\text{C}$  [9]. However, the fringe peak/dip identification remains a difficulty in many situations. Today, fiber temperature sensors combined with various materials have improved the sensitivity, but the problems of low resolution and direction ambiguity have not been solved.

In this Letter, a novel micro-tip temperature sensor is reported, which is based on a fiber probe with a tapered hollow capillary tube (HCT) that filled with the glycerin and the dye-doped cholesteric liquid crystal (DDCLC). The cholesteric liquid crystal (CLC) can be considered as a mirrorless photonic bandgap (PBG) microcavity [10]. When the DDCLC pumped by a pulsed laser that coupled into the fiber, a sharp PBG mode single peak appears in the reflection emission spectra of the sensor. Furthermore, we have proposed and experimentally demonstrated a simple, effective, and integrable laser emission method for the first time, to the best of our knowledge. This approach does not require sophisticated laser alignment and acquisition devices. While the LC laser is excited by pump light, the lasing emission spectra are also collected by the multimode fiber (MMF) coupler; this is quite meaningful in the field of fiber-tunable lasers.

The fabrication process of the proposed fiber-tip temperature sensor is shown in Fig. 1. Figures 1(a), 1(c), 1(e), and 1(g) are

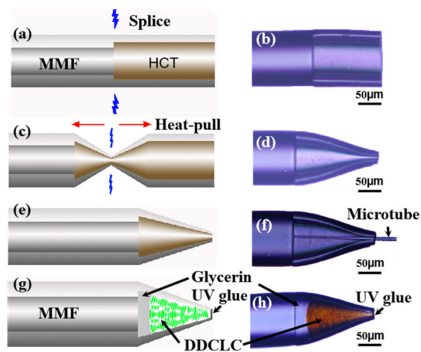


**Fig. 1.** Fabrication process of a fiber-tip temperature sensor. (a) and (b) Splices of the HCT to the MMF. (c) Fusion tapering of the HCT. (d) and (e) Images of the tapered HCT. (f) Inject glycerin and DDCLC into the tapered HCT. (g) Schematic diagram of the fiber-tip temperature sensor. (h) Microscope image of the fiber-tip temperature sensor. The scale bar is 50  $\mu\text{m}$ .

schematic diagrams of the manufacturing process of the tapering HCT, and Figs. 1(b), 1(d), 1(f), and 1(h) are microscope images of the tapering HCT. In the first step, a segment of HCT with the outer diameter of 150  $\mu\text{m}$  and the inner diameter of 75  $\mu\text{m}$  is spliced to a MMF with the core diameter of 62.5  $\mu\text{m}$  by using a fusion splicer, as shown in Figs. 1(a) and 1(b). In the next step, as shown in Fig. 1(c), the tapered HCT is fabricated by stretching the HCT while it is being heated with the electrode of the fusion splicer (FSM-80S, from Fujikura). The discharge time is 10 ms, discharge intensity 3 units. Then the stretched tapered HCT is cut into two parts under a microscope, and the image of the cut tapered HCT is shown in Figs. 1(d) and 1(e). The glycerin and the DDCLC are injected into the tapered HCT by a finer microtube (about 10  $\mu\text{m}$ ), respectively. The microtube is made by flame heating and tapering technology, and the microtube is connected to a needle tube and allows fluid to be freely drawn or injected in Fig. 1(f). The volume of the glycerin occupies 30.3% of the whole tapered HCT. The CLC is prepared by doping 28 wt. % S811 chiral dopant into the nematic LC (TEB30A,  $n_e = 1.692$ ,  $n_o = 1.522$ ,  $C_p = 61^\circ\text{C}$ ,  $M_p = -10^\circ\text{C}$ ). (All materials are from BayiSpace, China.)  $C_p$  is the clearing point temperature of LCs, and  $M_p$  is the melting point of LCs. Laser dye 4-dicyano-methylene-2-methyl-(6-4-dimethylaminostryl)-4 H-pyran ([DCM], from Exciton) with a concentration of 1 wt% is added into the CLC as a gain medium in all experiments in this Letter. Finally, the fiber-tip temperature sensor is encapsulated in UV curing adhesive. The length of the tapering HCT is about 200  $\mu\text{m}$ . The inner diameter of the HCT connecting the fiber end face is 75  $\mu\text{m}$ . The thinnest part is about 25  $\mu\text{m}$ , and the inner diameter is about 10  $\mu\text{m}$ , as shown in Figs. 1(g) and 1(h). The tapered HCT structure not only increases the stability of the structure and makes it easy to encapsulated, but also reduces the size of the fiber-tip sensor, allowing for a smaller-scale temperature measurements.

The configuration of the experimental system is shown in Fig. 2. A frequency-doubled Nd:YAG pulsed laser (532 nm, 8 ns pulse duration, and 5 Hz repetition rate) is employed as the pumping source. The pumping laser passes through an objective lens (40 $\times$ ); then it is coupled into one of the input ports of the MMF coupler. The output port of the coupler is connected to the fiber-tip temperature sensor which is located in a warm box with a resolution of 0.1 $^\circ\text{C}$ . The spectrum of the

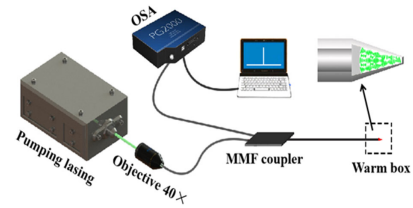


**Fig. 2.** Schematic of the experimental setup for the temperature sensor.

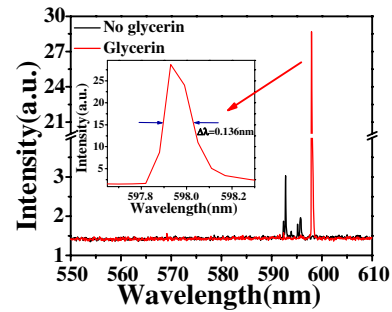


**Fig. 3.** Comparison of the emission spectra of the fiber-tip temperature sensor with (red line) and without (black line) glycerin. The inset shows the expanded spectrum in the range of 597–598 nm for identifying the line width.

excited DDCLC laser is collected and transmitted by MMF, and measured by an optical spectrum analyzer (PG2000, the spectral resolution is 0.04 nm).

Since glycerin provides a surface anchoring force to control the uniform orientation of CLC molecules, when the DDCLC is filled into the tapered HCT that has been partially filled with glycerin, the DDCLC can self-assemble into a radial internal structure in 10 min [11]. As a result, the DDCLC with a radial periodic structure can be seen as a Bragg resonator cavity. According to the principle of Bragg reflection, the CLC can selectively reflect light when the wavelength  $\lambda_c = \bar{n}p$  [12], where  $\bar{n}$  is the average refractive index of LC and  $p = 1/(\beta c)$  is the helical pitch,  $c$  is the concentration of the chiral dopant, and  $\beta$  is the helical twisting power. The positions of the wavelength edges of the reflection band are  $\lambda_1 = n_e p$  and  $\lambda_2 = n_o p$ , respectively. The lasing in the planar CLC cell is the photonic bandedge lasing [13]. The laser peak appears either on the short or the long edge of the PBG, depending on where the dye has the optimal gain. The optical gain material used in our experiments is DCM which has a fluorescence emission wavelength of about 600 nm. Only when the wavelength edge of the reflection band is close to the DCM fluorescence emission wavelength are the edges of the reflection band amplified and the PBG generated. The positions of the short-wavelength edges of the reflection band are far from the gain region of the DCM in our experiments. Thus, the reflection emission spectra of the temperature sensing probe have only a sharp long-wavelength bandedge lasing emission peak, as shown in the red line of Fig. 3.

The single PBG mode peak with high intensity and ultra-narrow line width ( $\Delta\lambda = 0.136$ ) is excellent for fiber-optic sensing. The black line presents resonance spectra of the fiber-tip sensor without glycerin. Since the HCT has no surface anchoring abilities, and the CLC molecules exhibit a chaotic

arrangement. The emission spectra show multiple resonance peaks with low intensity, and this is not conducive to temperature detection. Therefore, it is necessary to add glycerin as an orientation material to the fiber-tip sensor. In addition, we also use polyvinyl alcohol (PVA) solution and photo-alignment polyimide (PI) as the orientation material. However, the PVA solution is easily dehydrated and causes capillary blockage. The PI films need to be exposed in polarized ultraviolet light, and the orientation effect is not very good.

The temperature sensitivity of the sensor is tested by varying the surrounding temperature of the warm box. Since the refractive index of LCs is well known for its excellent response to temperature, the wavelength of the PBG mode changes when the refractive index of LCs varies, and the temperature-dependent LCs refractive indices can be described by [14]

$$\frac{dn_e}{dT} = -B - \frac{2\beta(\Delta n)_o}{3T_c \left(1 - \frac{T}{T_c}\right)^{1-\beta}}, \quad (1)$$

where  $-B$  is a constant for a given material,  $\beta$  is an exponent,  $T_c$  is the clearing temperature of the LC, and  $\Delta n = n_e - n_o$ . From Eq. (1), we can find that  $n_e$  decreases as the temperature increases. Additionally, the pitch has a slight increase in our temperature range [15]. The wavelength of the long-wavelength bandedge lasing mode is given by  $\lambda = n_e p$ . Therefore, in theory, it is clear that the wavelength  $\lambda$  of the PBG mode peak decreases as the temperature increases. In general, the change in  $n_e$  of LC with temperature is nonlinear, but it can be seen as linear over a specific temperature range [16].

Figure 4(a) presents the emission spectra of the fiber-tip temperature sensor at different temperatures. It is shown that the emission spectra exhibited a blueshift when the temperature increased from 23°C to 29°C. A wider temperature sensing range can be obtained by adopting different kinds of LCs, and the temperature measurement range can be changed by using a chiral dopant of different concentrations [17]. When the temperature is 23°C, the resonant peak wavelength of the PBG mode appears at 637.79 nm. As the temperature increases to 29°C, the resonant peak wavelength of the PBG mode blue shifts to 581.50 nm. Resonant peak wavelengths have a near linear relationship with temperature, and the temperature sensitivity of the fitting is  $-9.167 \text{ nm/}^\circ\text{C}$ . Additionally, the linearity of the fitting line is above 0.992. The resonant peak wavelength of the PBG mode still near linear shift with the decreasing of the temperature in the range from 29°C to 23°C, and the temperature sensitivity reached  $-8.814 \text{ nm/}^\circ\text{C}$ . Additionally, the linearity of the fitting line is also above 0.992, as shown in Fig. 4(b). When compared with other sensors, it is convenient to refer to the figure of merit (FOM) [18], which could be expressed as an equation ( $\text{FOM} = S/L_W$ ). Here  $S$  is the sensitivity of the sensor, and  $L_W$  is the line width of its spectrum. The FOM is an important criterion for the quality of the sensor. The proposed sensor has a very high FOM (67.4), which is much larger than other optical fiber-based temperature sensors, as shown in detail in Table 1. This temperature sensitivity is better than that of most reported fiber temperature sensors.

Stability is one of the important parameters of testing temperature sensitive properties. Figure 4(c) illustrates a characteristic resonant peak wavelength response of the proposed sensor

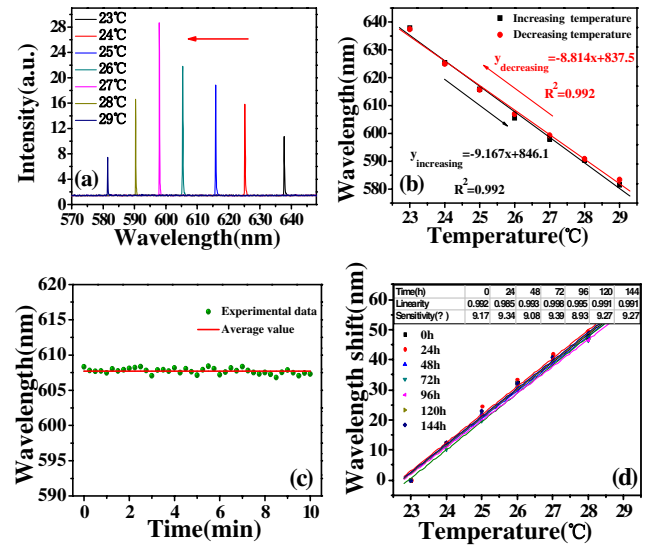


**Fig. 4.** (a) Emission spectra of the fiber-tip temperature sensor at different temperatures. (b) Resonant wavelength of the PBG mode as a function of temperature. (c) Change of the resonant peak wavelength with pumping time at a lasing frequency of 5 Hz. (d) Sensitivity changes of the fiber-tip sensor are measured every 24 h in a week.

versus time under 27°C, and the pumping laser is used continuously for 10 minutes with a pumping lasing frequency of 5 Hz. The average deviation of the proposed sensor is 0.30 nm. The sensitivity changes of the sensor are also measured every 24 h. The average sensitivity of the proposed sensor is  $9.21 \text{ nm/}^\circ\text{C}$ , the maximum sensitivity is  $9.39 \text{ nm/}^\circ\text{C}$ , and the sensitivity deviation is 1.9%, as shown in Fig. 4(d). Since the resolution of the used warm box only has  $0.1^\circ\text{C}$ , for the sensitivity of this sensor, a small temperature change can cause a large spectral shift. We think the error comes from the temperature fluctuation of the warm box.

Furthermore, different kinds of LCs have different temperature characteristics; in order to meet different requirements of temperature sensing in various application areas, two additional LCs are adopted. Figure 5(a) shows the temperature dependence of the PBG mode peak wavelength of CLC1 (BHR32400-200,  $n_e = 1.765$ ,  $n_o = 1.514$ ,  $C_p = 104^\circ\text{C}$ ,  $M_p = -40^\circ\text{C}$  and doping 28 wt. % S811 chiral dopant). From Eq. (1), we can find that  $n_e$  decreases as the temperature increases, and the pitch of the CLC remains stable within a certain temperature range. After that, the pitch increases rapidly with temperature rises, and when a certain temperature is reached, the pitch decreases rapidly. This is because the pitch of the CLC will expand as the temperature rises after reaching a certain temperature. There were some differences in the temperature range of different CLCs. According to  $\lambda_1 = n_e p$ , the PBG mode peak wavelength of the CLC1 blueshifts with the increasing of the temperature in the range from  $21^\circ\text{C}$  to  $30^\circ\text{C}$ , redshifts as the temperature increases from  $30^\circ\text{C}$  to  $54^\circ\text{C}$ , and then blueshifts again with the increasing of the temperature. The red line in Figure 5(a) presents the resonant wavelength of the PBG mode as a local linear fitting of temperature from  $36^\circ\text{C}$  to  $54^\circ\text{C}$ . The temperature sensitivity of the fit is  $0.373 \text{ nm/}^\circ\text{C}$ . Additionally, the linearity of the fitting line is above 0.996. The temperature dependence of the PBG mode peak wavelength of CLC2 (DZS-001,  $n_e = 1.777$ ,  $n_o = 1.517$ ,  $C_p = 110^\circ\text{C}$ ,  $M_p = -10^\circ\text{C}$ , and

**Table 1. Comparisons between the Optical Fiber Temperature Sensors**

Structure	Temperature Sensitivity	Line Width	FOM (1/°C)	Reference
Long period fiber grating	55 pm/°C	~4 nm	0.0138	[19]
Mach-Zehnder interferometer	109 pm/°C	~5 nm	0.0218	[20]
WGM based on CLCs	0.96 nm/°C	1 nm	0.96	[21]
Liquid-air cavities based on Vernier effect	39.21 nm/°C	~50 nm	0.7842	[22]
PBG mode probe	9.167 nm/°C	0.136 nm	67.404	Our work

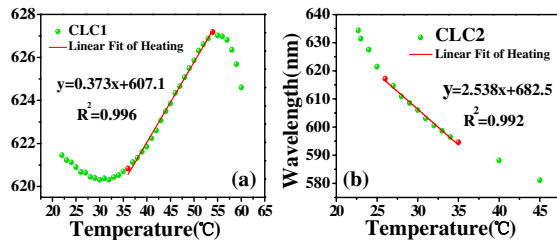


**Fig. 5.** (a) Temperature dependence of the PBG mode peak wavelength of CLC1, and the red line is a local linear fitting of temperature from 36°C to 54°C. (b) Temperature dependence of the PBG mode peak wavelength of CLC2, and the red line as a local linear fitting of temperature from 26°C to 35°C.

doping 26 wt. % S811 chiral dopant) is shown in Fig. 5(b). The  $n_e$  of the CLC2 decreases faster than CLC1 as the temperature increases. Therefore, the PBG mode peak wavelength of the CLC2 blueshifts with the increasing of the temperature, but the speed of the blueshift gradually decreases due to the pitch increasing with temperature rises. The red line in Figure 5(b) presents the resonant wavelength of the PBG mode as a local linear fitting of temperature from 26°C to 35°C. The resonant wavelengths have a near linear relationship with temperature, and the PBG mode temperature sensitivity of the fit is  $-2.538$  nm/°C; the linearity of the fitting line reaches 0.992. Under the condition of reduced sensitivity, adopting different kinds of LCs is also a good choice for expanding the temperature range. Furthermore, such a fiber-tip temperature sensor probe can meet different requirements of temperature sensing in various application areas by reasonable using different kinds of CLCs.

In conclusion, a novel, miniature fiber-tip temperature sensor with a tapered HCT that filled with the glycerin and DDCLC is reported in this Letter. The DDCLC in the tapered HCT can be considered as a Bragg cavity by using glycerin to control the parallel anchoring of the CLC molecules on the surface between CLC and glycerin. Therefore, a highly recognizable PBG mode single peak appears in the reflection emission spectra of the sensor. The temperature sensor based on the unambiguously identifiable PBG mode single peak has a temperature sensitivity of  $-9.167$  nm/°C, and the FOM is much larger than other optical fiber-based temperature sensors. The temperature sensitivity is also better than most reported fiber temperature sensors, to the best of our knowledge. The proposed CLC-based fiber-tip temperature sensor with high sensitivity and FOM is compact, stable, unambiguously identifiable, and biocompatibility, which exhibits a promising future for various temperature

sensing application fields. In addition, it has great potential in lasers and tunable optical devices.

**Funding.** National Science Foundation of China (U1531102, 61107059); Fundamental Research Funds for the Central Universities, National Natural Science Foundation of Heilongjiang (A2018002); Science and Technology on Vacuum Technology and Physics Laboratory, Lanzhou Institute of Physics (ZWK1801).

**Disclosures.** The authors declare no conflicts of interest.

## REFERENCES

- H. Li, H. Yang, E. Li, Z. Liu, and K. Wei, *Opt. Express* **20**, 11740 (2012).
- B. Y. Song, J. Y. Hu, C. L. Xia, H. Zhang, Y. L. Lu, W. M. Sun, and Y. J. Liu, *Appl. Opt.* **58**, 410 (2019).
- Q. H. Wang, H. Zhang, and D. N. Wang, *Opt. Lett.* **44**, 5145 (2019).
- Z. G. Liu, G. G. Liu, Y. P. Zhu, Q. W. Sheng, X. Wang, Y. Liu, Z. G. Jing, W. Peng, and M. Han, *J. Lightwave Technol.* **37**, 4210 (2019).
- C. Wu, H. Y. Fu, K. K. Qureshi, B. O. Guan, and H. Y. Tam, *Opt. Lett.* **36**, 412 (2011).
- J. Li, Q. Nie, L. Gai, H. Li, and H. Hu, *J. Lightwave Technol.* **35**, 3706 (2017).
- M. Li, Y. Liu, R. X. Gao, Y. Li, X. L. Zhao, and S. L. Qu, *Sens. Actuators, B* **233**, 496 (2016).
- D. J. J. Hu, J. L. Lim, Y. Cui, K. Milenko, and Y. Wang, *IEEE Photonics J.* **4**, 1248 (2012).
- F. R. Wang, Y. J. Liu, Y. L. Lu, L. L. Zhang, J. Ma, L. Wang, and W. M. Sun, *Opt. Lett.* **43**, 5355 (2018).
- J. Y. Hu, C. L. Xia, D. Y. Fu, C. Zhang, L. S. Yao, C. L. Lu, W. M. Sun, and Y. J. Liu, *Appl. Phys. Express* **12**, 102017 (2019).
- F. Xu and P. P. Crooker, *Phys. Rev. E* **56**, 6853 (1997).
- Y. Zhou, Y. Huang, and S. T. Wu, *Opt. Express* **14**, 3906 (2006).
- H. Coles and S. Morris, *Nat. Photonics* **4**, 676 (2010).
- Y. L. Lu, Y. Yang, Y. Wang, L. Wang, J. Ma, L. L. Zhang, W. M. Sun, and Y. J. Liu, *Opt. Express* **26**, 3277 (2018).
- M. F. Moreira, I. C. S. Carvalho, W. Cao, C. Bailey, B. Taheri, and P. Palffy-Muhoray, *Appl. Phys. Lett.* **85**, 2691 (2004).
- J. Li, S. Gauzia, and S. T. Wu, *Opt. Express* **12**, 2002 (2004).
- Y. Huang, Y. Zhou, C. Doyle, and S. T. Wu, *Opt. Express* **14**, 1236 (2006).
- A. Shalabney and I. Abdulhalim, *Opt. Lett.* **37**, 1175 (2012).
- T. T. Yuan, X. Zhong, C. Y. Guan, J. N. Fu, J. Yang, J. H. Shi, and L. B. Yuan, *Opt. Express* **23**, 33378 (2015).
- L. Jiang, J. Yang, S. Wang, B. Li, and M. Wang, *Opt. Lett.* **36**, 3753 (2011).
- L. Y. Zhao, Y. Wang, Y. G. Yuan, Y. J. Liu, S. Q. Liu, W. M. Sun, J. Yang, and H. Y. Li, *Opt. Commun.* **402**, 181 (2017).
- C. P. Lang, Y. Liu, Y. Y. Liao, J. J. Li, and S. L. Qu, *IEEE Sens. J.* **20**, 5286 (2020).